cmgh
CELLULAR AND MOLECULAR GASTROENTEROLOGY AND HEPATOLOGY

ORIGINAL RESEARCH

Overexpressed Claudin-1 Can Be Visualized Endoscopically in Colonic Adenomas In Vivo

Emily F. Rabinsky,[1] Bishnu P. Joshi,[1] Asha Pant,[1] Juan Zhou,[1] Xiyu Duan,[2] Arlene Smith,[1] Rork Kuick,[3] Shuling Fan,[4] Asma Nusrat,[4] Scott R. Owens,[4] Henry D. Appelman,[4] and Thomas D. Wang[1,2,5]

[1]Department of Medicine, Division of Gastroenterology, [2]Department of Biomedical Engineering, [3]Department of Biostatistics, [4]Department of Pathology, [5]Department of Mechanical Engineering, University of Michigan, Ann Arbor, Michigan

SUMMARY

Claudin-1 is highly overexpressed in human colonic adenomas. By using a near-infrared labeled fluorescent peptide, we show real-time in vivo images in a mouse model of spontaneous adenomas to show feasibility for future clinical translation to detect precancerous lesions.

BACKGROUND & AIMS: Conventional white-light colonoscopy aims to reduce the incidence and mortality of colorectal cancer (CRC). CRC has been found to arise from missed polypoid and flat precancerous lesions. We aimed to establish proof-of-concept for real-time endoscopic imaging of colonic adenomas using a near-infrared peptide that is specific for claudin-1.

METHODS: We used gene expression profiles to identify claudin-1 as a promising early CRC target, and performed phage display against the extracellular loop of claudin-1 (amino acids 53–80) to identify the peptide RTSPSSR. With a Cy5.5 label, we characterized binding parameters and showed specific binding to human CRC cells. We collected in vivo near-infrared fluorescence images endoscopically in the CPC;Apc mouse, which develops colonic adenomas spontaneously. With immunofluorescence, we validated specific peptide binding to adenomas from the proximal human colon.

RESULTS: We found a 2.5-fold increase in gene expression for claudin-1 in human colonic adenomas compared with normal. We showed specific binding of RTSPSSR to claudin-1 in knockdown and competition studies, and measured an affinity of 42 nmol/L and a time constant of 1.2 minutes to SW620 cells. In the mouse, we found a significantly higher target-to-background ratio for both polypoid and flat adenomas compared with normal by in vivo images. On immunofluorescence, we found significantly greater intensity for human adenomas (mean ± SD, 25.5 ± 14.0) vs normal (mean ± SD, 9.1 ± 6.0) and hyperplastic polyps (mean ± SD, 3.1 ± 3.7; $P = 10^{-5}$ and 8×10^{-12}, respectively), and for sessile serrated adenomas (mean ± SD, 20.1 ± 13.3) vs normal and hyperplastic polyps ($P = .02$ and 3×10^{-7}, respectively).

CONCLUSIONS: Claudin-1 is overexpressed in premalignant colonic lesions, and can be detected endoscopically in vivo with a near-infrared, labeled peptide. *(Cell Mol Gastroenterol Hepatol 2016;2:222–237; http://dx.doi.org/10.1016/j.jcmgh.2015.12.001)*

Keywords: Colon Cancer; Early Detection; Molecular Imaging.

Colorectal cancer (CRC) is one of the most common causes of cancer-related mortality worldwide.[1] Adenomatous polyps are precursor lesions[2] and may express early molecular targets that can be developed for imaging to improve methods of detection and cancer prevention. Conventional white-light colonoscopy is the preferred method for screening, and is one of the most frequently performed procedures in the United States.[3] However, the miss rate for grossly visible polyps can be up to 25% or higher.[4–6] Also, clinical studies have shown that colonoscopy confers a reduction in mortality from left-sided (distal) lesions, but much less so for right-sided (proximal) disease.[7–12] Right-sided lesions tend to be smaller in size, have more nonpolypoid (flat) features, and are more difficult to visualize.[13] Furthermore, flat adenomas may represent more than 35% of all premalignant lesions[14] and may result in preventable cancers.[15] Moreover, adenomas, which are premalignant, cannot be distinguished from hyperplastic polyps, which have no malignant potential.[16] Sessile serrated adenomas (SSAs) tend to be flat in appearance, and can result in more than 17.5% of proximal colon cancers.[17]

Claudin-1 is an integral membrane protein with 4 membrane-spanning regions and 2 extracellular loops that form tight junctions between epithelial cells to maintain cell polarity and regulate paracellular transport.[18] This protein is overexpressed in several human cancers, including colorectal,[19–22] pancreas,[23] cervical,[24] squamous cell,[25] stomach,[26] nasopharyngeal,[27] and thyroid.[28] From gene

Abbreviations used in this paper: **APC, adenomatous polyposis coli; BSA, bovine serum albumin; CLDN1, claudin-1; CRC, colorectal cancer; DAPI, 4′,6-diamidino-2-phenylindole; HRP, horseradish peroxidase; IF, immunofluorescence; IHC, immunohistochemistry; PBS, phosphate-buffered saline; PBST, phosphate-buffered saline plus 0.1% Tween-20; PFA, paraformaldehyde; RT, room temperature; siCL, control small interfering RNA; siRNA, small interfering RNA; SSA, sessile serrated adenoma; T/B, target-to-background; TEER, transepithelial electrical resistance; TFA, trifluoroacetic acid; ZO-1, zonula occludens-1.**

Most current article

2352-345X
http://dx.doi.org/10.1016/j.jcmgh.2015.12.001

expression analysis, claudin-1 is increased by more than 40-fold in adenocarcinoma compared with normal colon.[29] This cell surface target also has been found to be overexpressed in SSAs.[30] Claudin-1 overexpression in neoplasia is believed to increase cell proliferation, motility, and invasiveness, and may contribute to the loss of cell polarity, abnormal cellular organization, and decreased differentiation.[31,32] Claudin-1 also has been found to have increased expression in neoplasia associated with inflammatory bowel disease.[33–35]

Peptides have shown promise for clinical use to detect overexpressed cell surface targets during endoscopy.[36,37] Peptides show high binding affinity, with rapid binding onset, and are inexpensive to mass manufacture. In addition, high peptide concentrations can be used with topical administration to colonic mucosa to maximize the binding interactions and achieve optimal image contrast with minimal risk for toxicity.[38] Because of the large diversity of sequences possible, the specificity of peptides can be very high, and nanomolar binding affinities can be achieved.[39] Peptides have flexibility to be optically labeled with a broad range of fluorophores for use in multiplexed imaging strategies to address tumor heterogeneity.[40] Peptides with short amino acid sequences have minimal immunogenicity because of their specific small size (<1 kilodalton), and can be arranged in a multimer configuration to improve detection sensitivity and increase specificity and avidity from a multivalency effect.[41] Here, we aimed to show real-time endoscopic imaging of overexpressed claudin-1 in both polypoid and flat adenomas in vivo to establish proof-of-concept for future clinical translation as an early molecular target for detection of CRC.

Methods

Identification of Claudin-1 Target

We evaluated the GSE41258 gene expression data set to identify promising early targets for imaging that are overexpressed in colonic adenomas compared with normal.[29] We analyzed 22,283 probe-sets using the Affymetrix (Santa Clara, CA) HG_U133A array platform. Data from N = 52 normal and N = 45 adenomas were selected. Two-sample *t* tests and average fold-changes were computed. Data were evaluated based on the following criteria: *P* value less than 10^{-5}, average fold-change greater than 2, and location on plasma membrane using Gene Ontology terms obtained from Affymetrix (ver na32).

Materials

We used human colorectal adenocarcinoma cell lines SW620, SW480, and HCT116 (American Type Culture Collection, Manassas, VA). SW620 and SW480 cells were cultured in Dulbecco's modified Eagle medium and HCT116 cells were cultured in McCoy's 5a medium using a 37°C humidified incubator with 5% CO_2. All cell culture media (Gibco, Carlsbad, CA) were supplemented with 10% fetal bovine serum and 1% penicillin/streptomycin.

Identification of a Peptide Specific for Claudin-1

We performed phage display with a PhD7 library (New England Biolabs, Ipswich, MA) using the claudin-1 (CLDN1) extracellular loop mimetic peptide CLDN-$1_{53–80}$ with a biotinylated C-terminus (Biomatik, Cambridge, Ontario) as the target. Biopanning was performed per the manufacturer's guidelines using 15-mm dishes coated with 0.1 mg/mL streptavidin, washed with Tris-buffered saline with 0.1% Tween-20, and blocked for 1 hour at 4°C with blocking buffer consisting of 0.1 mol/L $NaHCO_3$ with 0.5% bovine serum albumin (BSA) and 0.1 μg/mL streptavidin. The phage library (1×10^{11} pfu containing 1.28×10^9 unique 7 amino acid sequences with 100 copies) was first cleared of nonspecific binders by biopanning against 2 streptavidin-coated dishes and 1 uncoated dish for 30 minutes at room temperature (RT) with agitation. Unbound phages were collected after each clearing step and used in the following rounds. After 3 rounds of clearing, the remaining phages were amplified to 2×10^{11} for biopanning with the claudin-1 target in a blocked streptavidin-coated dish for 30 minutes at RT. Biotin at a final concentration of 0.1 mmol/L was added for 5 minutes to bind any free streptavidin. The dishes were washed 10× with Tris-buffered saline with 0.1% Tween-20 and weak binders were removed by eluting with 0.2 mol/L glycine, pH 2.2, with 1 mg/mL BSA for 2 minutes. A second elution was performed for 13 minutes to remove strong binders and was incubated with neutralization buffer (1 mol/L Tris-HCl, pH 9.1), amplified, and titered for the next round of biopanning. Three rounds of biopanning were performed with decreasing concentrations of biotinylated claudin-1 extracellular loop mimetic peptide (75, 50, and 25 nmol/L) and were incubated with 2×10^{11} phages for decreasing periods of time (60, 40, and 20 minutes, respectively) to improve specificity. The concentration of Tween-20 was increased from 0.1% to 0.5% in the washing buffer in rounds 2 and 3. The unamplified eluate from the strong binders in round 3 was titered overnight and 50 plaques were selected for DNA sequencing.

Peptide Synthesis

The RTSPSSR (RTS*) phage was found to be highly enriched (43 of 50 clones) after 3 rounds. This sequence was scrambled as SPTSSRR (SPT*) for use as control. The peptides were synthesized using standard solid-phase 9-fluorenylmethyloxycarbonyl chemistry, and labeled at the C-terminus with Cy5.5 using a 5–amino acid linker GGGSK. All chemicals and reagents used were analytic grade (Sigma-Aldrich, St. Louis, MO), unless otherwise noted. Reagents for peptide synthesis (Anaspec, Fremont, CA and AAPPTEC, Louisville, KY) had more than 99% purity and were used without further purification. Synthesis of both peptides was performed with a PS3 automatic synthesizer (Protein Technologies, Inc, Tucson, AZ) using t-butyloxycarbonyl and 9-fluorenylmethyloxycarbonyl protected *L*-amino acids before manually labeling with the dye. Upon completion of synthesis, the 1-(4,4-Dimethyl-2,6-dioxocyclohexylidene)-3-methylbutyl side chain was removed with 5% hydrazine in dimethylformamide with agitation for 20 minutes at RT 3×. The resin-linked peptide then was washed 3× with dimethylformamide and dichloromethane. The Cy5.5 fluorophore (Lumiprobe, Hallandale Beach, FL) was added along with di-isopropylethylamine and incubated

for 24–48 hours with agitation at RT. The peptide then was cleaved from the resin with chilled trifluoroacetic acid (TFA):triisopropylisilane:water (9.5:0.25:0.25, vol/vol/vol, respectively) for 4 hours with agitation at RT. The peptides were separated from the resin and cleavage cocktail was evaporated with N_2 gas before precipitating the peptide with diethyl ether in an overnight incubation at -20°C. The precipitate was collected by centrifugation at 1780×g for 5 minutes and suspended in acetonitrile:water (1:1, vol/vol, respectively). Both peptides were purified to more than 95% via high-performance liquid chromatography (Waters, Milford, MA) using a water (0.1% TFA)-acetonitrile (0.1% TFA) gradient. The mass-to-charge ratio of the Cy5.5-labeled peptides was measured using mass spectrometry.

Immunocytochemistry

SW620, SW480, and HCT116 cells were added to 12-well plates at a density of 0.5 × 10^6 cells/mL. The following day, they were fixed with ice-cold methanol for 20 minutes at -20°C, blocked with phosphate-buffered saline (PBS) plus 2% BSA for 1 hour at RT, then incubated first with the primary anti-CLDN1 antibody (clone Jay.8; Invitrogen, Carlsbad, CA) at 5 μg/mL at 4°C overnight, then with (1:500) goat anti-rabbit secondary antibody labeled with Alexa Fluor 488 (AF488; Life Technologies, Grand Island, NY) for 1 hour at RT. Finally, cells were counterstained with 4′,6-diamidino-2-phenylindole (DAPI) + Prolong Gold (Thermo Fisher Scientific, Waltham, MA) before being mounted on slides and imaged with a Leica (Wetzlar, Germany) SP5x confocal microscope using a 63× (numeric aperture, 1.4) oil-immersion objective.

Small Interfering RNA Knockdown of Claudin-1 Expression

CLDN1 expression was knocked down using Dharmacon On-Target Plus SMARTpool Human CLDN1 small interfering RNA (siRNA) (Thermo Fisher Scientific) per the manufacturer's protocol. SW620 cells were plated overnight on coverslips in a 12-well plate at 0.2 × 10^6 cells/mL. The following day, the cells were transfected with 3 μL DharmaFECT1 and either 25 nmol/L CLDN1 or control siRNA. After 72 hours, the transfected cells were analyzed for claudin-1 expression. The cytoplasmic and plasma membrane fractions were extracted using a plasma membrane protein extraction kit (BioVision, Milpitas, CA). The total protein in the cytoplasmic and plasma membrane fractions were quantified using a bicinchoninic acid protein assay kit (Pierce, Thermo Fisher Scientific), and 3 μg total protein of each fraction were run on a Novex (Thermo Fisher Scientific) 4%–20% 1.5-mm protein gel before transferring to a polyvinylidene difluoride membrane. The membrane was blocked with PBS plus 0.1% Tween-20 (PBST) plus 5% nonfat milk for 1 hour at 4°C, stained with either rabbit anti-CLDN1 antibody or mouse antitubulin antibody (clone 2-28-33; Invitrogen) at 4°C overnight, then with anti-rabbit horseradish peroxidase (HRP) (1:500, for CLDN1) or anti-mouse HRP (1:500, for tubulin) for 1 hour at RT before developing. The transfected cells were lysed with radioimmunoprecipitation assay buffer containing mini-complete EDTA-free protease inhibitor (Roche) for 10 minutes on ice, collected, and spun at 20,000×g for 10 minutes at 4°C. The total protein concentration was quantified with the bicinchoninic acid assay, and 10 μg protein from each sample was run on a Novex 4%–20% 1.5-mm protein gel before transferring to a polyvinylidene difluoride membrane. The membrane was blocked with PBST + 5% nonfat milk for 1 hour at 4°C overnight, then with anti-rabbit HRP (1:500, for CLDN1) or anti-mouse HRP (1:500, for tubulin) for 1 hour at RT before developing.

For immunocytochemistry, the transfected cells were further passaged and grown on coverslips. Cells were fixed with ice-cold methanol for 20 minutes at -20°C, blocked for 1 hour at RT with PBS + 2% BSA, stained with anti-human CLDN1 antibody at 5 μg/mL for 1 hour at RT, then with goat anti-rabbit antibody labeled with AF488 (1:500) for 1 hour at RT, and then counterstained with DAPI + Prolong Gold. siRNA-transfected cells also were stained with 5 μmol/L RTS*-Cy5.5 or SPT*-Cy5.5 for 30 minutes at 4°C, and fixed with 4% paraformaldehyde for 10 minutes at RT.

Competition for Peptide Binding

SW620 cells were plated at approximately 0.5 × 10^6 cells/mL on coverslips in 12-well plates. The following day, the cells were treated first with unlabeled RTS* peptide at 0, 25, 50, 100, 200, or 400 μmol/L for 30 minutes at 4°C, washed with PBS, and then treated with 5 μmol/L RTS*-Cy5.5 for 30 minutes at 4°C. The cells were fixed with 4% PFA for 5 minutes at RT, washed, and counterstained with DAPI + Prolong Gold. Fluorescence intensities were quantified with custom software developed with Matlab (Mathworks, Natick, MA).

Cell Binding Assay

SW620, SW480, and HT29 cells were plated at approximately 0.5 × 10^6 cells/mL on coverslips on 12-well plates. The following day, the cells were treated with either 10 μmol/L RTS*-Cy5.5 or SPT*-Cy5.5 for 1 hour at 4°C, fixed with 4% PFA for 10 minutes at RT, then counterstained with DAPI + Prolong Gold. Fluorescence intensities from 10 randomly chosen cells in 3 independent images were quantified using custom software. Statistical analysis was performed using a 1-way analysis of variance with GraphPad Prism software (San Diego, CA).

Characterization of Peptide Binding

The apparent dissociation constant of RTS*-Cy5.5 to SW620 cells was measured. SW620 cells were washed 2× with PBS + 0.5% BSA, then approximately 10^5 cells were incubated with RTS*Cy5.5 at dilutions ranging from 0 to 200 nmol/L for 1 hour at 4°C. Cells then were washed of unbound peptide 5× with PBS + 0.5% BSA before analyzing with flow cytometry (FACS Canto; BD Biosciences, San Jose, CA). Sample means were used to calculate the equilibrium dissociation constant k_d using nonlinear regression analysis with GraphPad Prism software.[42]

To measure the apparent association time constant of RTS*-Cy5.5, SW620 cells were washed 2× with PBS + 0.5% BSA, then approximately 10^5 cells were incubated with

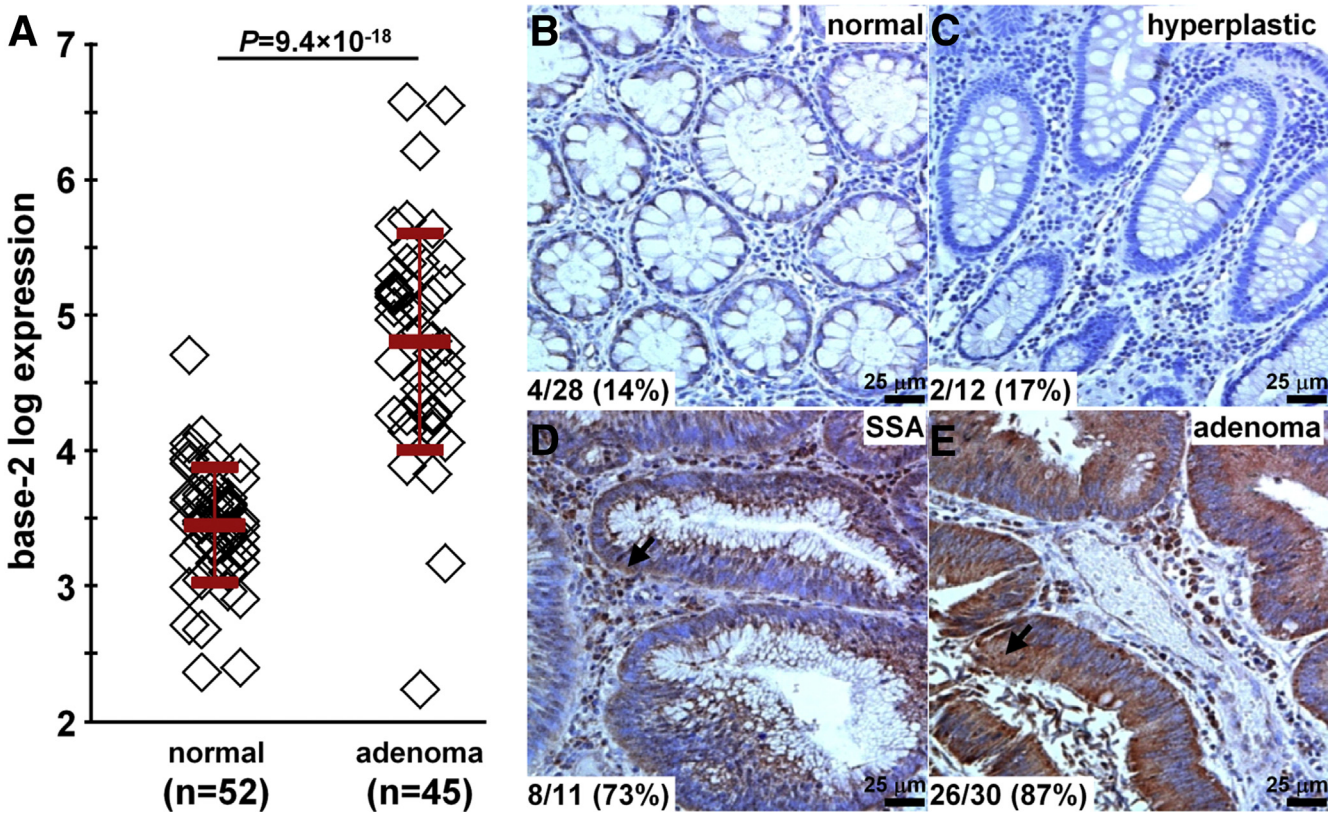

Figure 1. Claudin-1 is an early target for CRC. (*A*) From the GSE41258 gene expression data set, the mean (±SD) base-2 log level for claudin-1 was 4.8 ± 0.8 and 3.5 ± 0.4 for human adenomas (n = 45) and normal (n = 52) colonic mucosa, resulting in an average difference of 2.54-fold ($P = 9.4 \times 10^{-18}$) by 2-sample *t* test. On immunohistochemistry, minimal staining was observed from representative sections of (*B*) normal and (*C*) hyperplastic polyps. Intense cell surface staining (*arrows*) was seen in representative sections of (*D*) SSAs and (*E*) adenomas from human proximal colon specimens. By using a standard IHC scoring system, overexpression (2+/3+) of claudin-1 was found in 14% (4 of 28) of normal, 17% (2 of 12) of hyperplastic polyps, 73% (8 of 11) of SSAs, and 87% (26 of 30) of adenomas.

5 μmol/L RTS*-Cy5.5 at 4°C for time intervals ranging from 2 to 15 minutes. The cells were immediately washed of unbound peptide 5× with PBS + 0.5% BSA before analyzing with flow cytometry. The mean fluorescence intensity of SW620 cells at the various time points was set in a ratio with untreated cells and used to calculate the rate constant k by fitting the data to a first-order kinetics model, $y(t) = I_{max}\,[1 - \exp^{(-kt)}]$, using Origin 6.1 software (OriginLab Corp, Northampton, MA).[41]

Transepithelial Electrical Resistance Measurements

T84 human colon carcinoma cells were grown in a 1:1 mixture of Dulbecco's modified Eagle medium and Ham's F-12 culture medium supplemented with 5% fetal bovine serum. To establish a polarized monolayer, the cells were plated on Transwell permeable polyester supports (Corning Life Sciences, Tewksbury, MA) (1.12 cm^2; pore size, 3 μm; Costar) until they reached confluence after approximately 3–4 days, as determined by an increase in transepithelial electrical resistance (TEER).[43] The cells were continually grown on Transwell supports until the TEER reached approximately 2000 Ω-cm^2. Then, 5 μmol/L of either RTS-Cy5.5 or control peptides were added. TEER then was measured at 6, 12, and 24 hours. The cells were fixed with 4% PFA for 12 minutes. After brief washing, 1% sodium dodecyl sulfate in PBS was used to permeabilize the cells. These procedures were followed by 3% goat serum in PBS blocking for 30 minutes. Mouse anti–zonula occludens-1 (anti–ZO-1) (1:250; Life Technologies) and rabbit anti–claudin-1 (1:200; Life Technologies) antibodies were diluted in block buffer and incubated in a humidity box overnight at 4°C and fluorescent secondary antibodies were diluted to 1:1000 and incubated for 1 hour at RT.[44] All images were obtained using a Nikon (Melville, NY) A1 confocal microscope (Microscopy & Image Analysis Laboratory, University of Michigan).

In Vivo Imaging in Mouse Colon

We used a *CPC;Apc* mouse model of CRC in which the adenomatous polyposis coli (APC) allele sporadically is deleted by Cre recombinase in colonic epithelium,[45] resulting in spontaneous formation of flat and polypoid colonic adenomas. This model is representative of human disease because APC mutations are found in more than 80% of sporadic colorectal cancers.[46] We used a rigid small animal

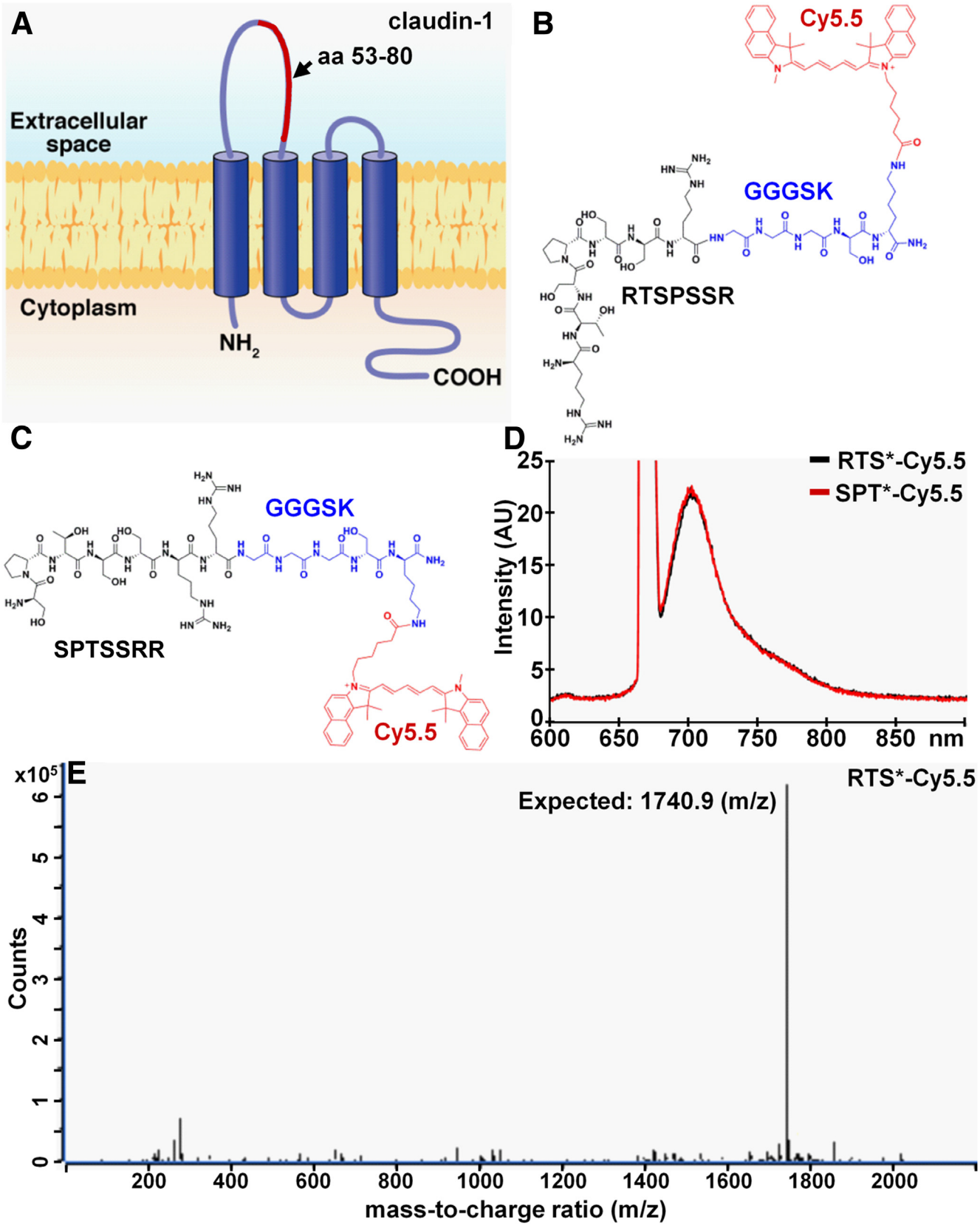

Figure 2. Peptide specific for claudin-1. (*A*) The extracellular loop of CLDN1, consisting of amino acids 53–80 (red), was used to select the (*B*) peptide with sequence RTSPSSR. The chemical structure of the peptide (black) with a GGGSK linker (blue) and Cy5.5 label (red) is shown. (*C*) Scrambled peptide with sequence SPTSSRR labeled with Cy5.5 is used as control. (*D*) Fluorescence spectra with $\lambda_{ex} = 671$-nm excitation shows peak emission in near-infrared at 710 nm for both peptides. (*E*) For RTS*-Cy5.5, the mass-to-charge (m/z) ratio of 1740.9 was measured on mass spectrometry, which agrees with the expected value.

endoscope (Karl Storz Veterinary Endoscopy-America, Goleta, CA) to image the distal 2 cm of colon.[47] The mouse studies were performed with approval of the University of Michigan Committee on the Use and Care of Animals. The mice were housed in pathogen-free conditions and supplied water ad libitum under controlled conditions of humidity (50% ± 10%), light (12-/12-hour light/dark cycle), and temperature (25°C). Anesthesia was induced and maintained via a nose cone with inhaled isoflurane mixed with oxygen at a concentration of 2%–4% at a flow rate of

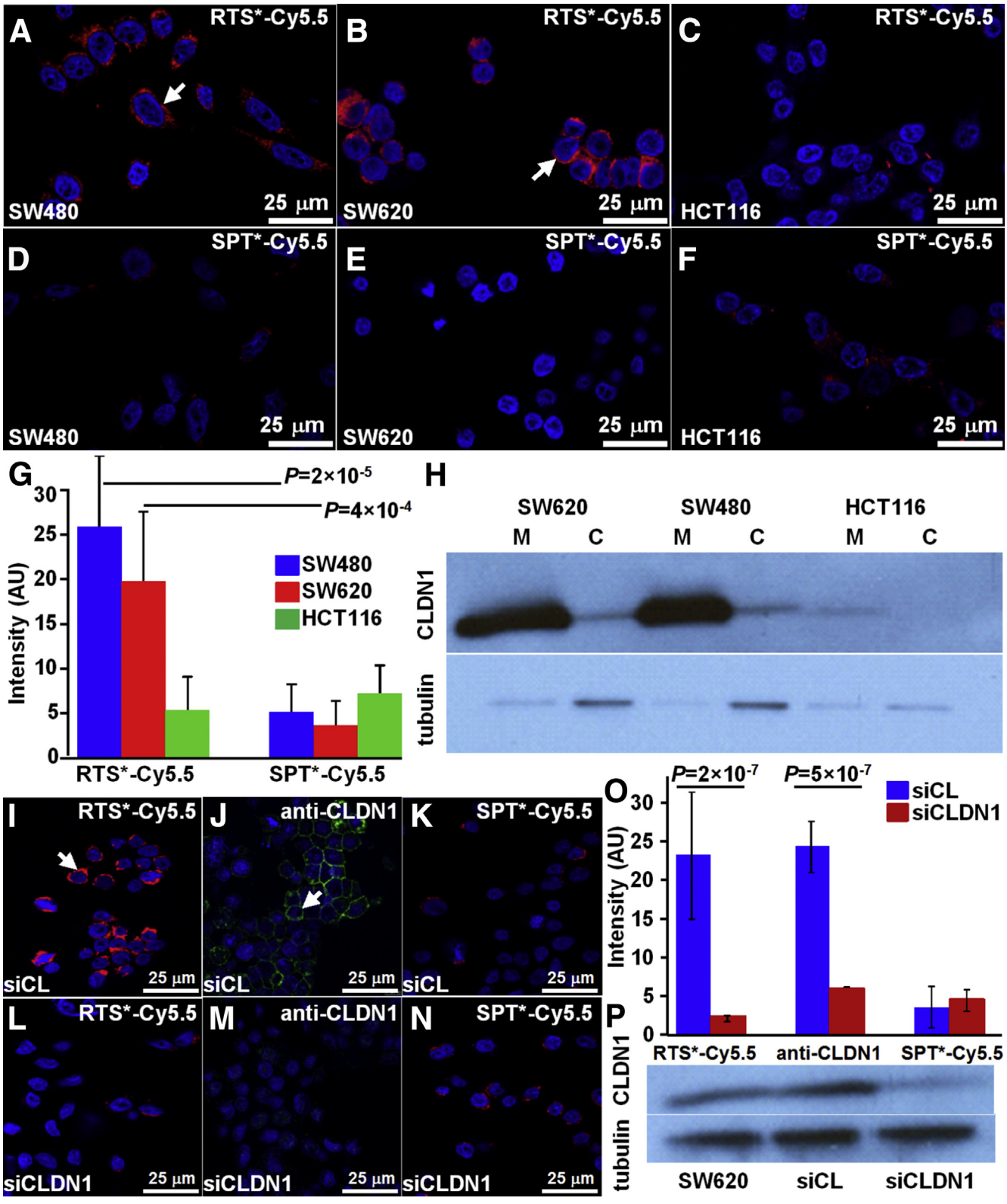

approximately 0.5 L/min. Mucus was removed by vigorously rinsing the colon with water. We used white-light illumination first to identify adenomas. A 100-μmol/L solution of RTS*-Cy5.5 was administered intrarectally, and allowed to incubate for 5 minutes before rinsing away the unbound peptides with water. The colon then was imaged with fluorescence. We recorded the following: (1) distance between the endoscope tip and the anus, and (2) clockwise location of each region of high intensity. Several days later, endoscopy was repeated to confirm that all residual signal from RTS*-Cy5.5 had disappeared, and then the mice were imaged with the SPT*-Cy5.5 control peptide. On the endoscopic images, we determined the average fluorescence intensity from 3 regions of interest with dimensions of 20 $\times$ 20 μm^2 picked at random from the regions of high fluorescence intensity (target) and adjacent areas of normal colonic mucosa (background) to measure the target-to-background (T/B) ratio.

After imaging completion, the mice were euthanized, and the colon was resected and divided longitudinally to expose the mucosal surface. We first collected white-light images using the Xenogen IVIS Spectrum (Caliper Life Sciences, Hopkinton, MA). Near-infrared fluorescence images then were collected using 675-nm excitation and 720-nm emission with 1-second exposure time. A ruler was placed next to the specimen to determine the distance from the anus for registration with the endoscopy and histology images. The specimen then was processed for histology by cutting sections in the plane parallel to the mucosal surface. Digital images were collected with a Zeiss (Jena, Germany) Axiovision microscope (Thornwood, NY) using 5$\times$ magnification, and stitched together using Image Composite Editor (Microsoft, Redmond, WA). A pathologist (S.R.O.) who was blinded to the imaging results reviewed the composite histology, and identified regions of dysplasia and normal colon. Fluorescence intensities from these sites were measured from 2 concentric ellipses of equal area using Living Image 4.0 software (Caliper Life Sciences). The inner and outer regions were used to define the target and background values, respectively.

Validation of Claudin-1 Expression in Mouse and Human Proximal Colon Specimens

Formalin-fixed specimens from mouse colon were deparaffinized. Antigen retrieval was performed using standard methods. Briefly, the sections were incubated 3$\times$ in xylene for 3 minutes, washed 2$\times$ with 100% ethanol for 2 minutes, and washed 2$\times$ with 95% ethanol for 2 minutes. Rehydration was performed by washing with distilled H_2O (dH_2O) for 5 minutes. Antigen unmasking was performed by boiling the slides in 10 mmol/L sodium citrate buffer with 0.05% Tween at pH 6.0, and then maintaining at a sub-boiling temperature for 15 minutes. The slides were cooled for 30 minutes. The sections were washed 3$\times$ with dH_2O for 3 minutes, and then incubated in 3% H_2O_2 in methanol for 10 minutes. The sections were washed 3$\times$ in dH_2O for 2 minutes and in PBST for 5 minutes.

Blocking was performed with protein blocking agent (X0909; Dako, Carpinteria, CA) for 15 minutes at RT. The blocking solution was washed 3$\times$ with PBS. For mouse specimens, we used primary rabbit polyclonal anti–claudin-1 antibody (ab 15098; Abcam, Cambridge, MA), and for human specimens, we used primary rabbit polyclonal anti–claudin-1 antibody (clone Jay.8, Invitrogen). The sections were incubated overnight at 4ºC in a humidified chamber and then washed 3$\times$ in PBST for 5 minutes. A 1:200 dilution of biotinylated secondary antibody (goat anti-rabbit IgG) was added to each section and incubated for 30 minutes at RT, and then removed by washing 3$\times$ with PBST for 5 minutes. Pre-mixed Elite Vectastain ABC reagent (Vector Labs, Burlingame, CA) was added to each section and incubated for 30 minutes at RT. The sections were washed 3$\times$ in PBS for 5 minutes, and developed with 3,3'-diaminobenzidine tetrahydrochloride substrate. The reaction was monitored for up to 5 minutes, and then quenched by immersing the slides in deuteriumH_2O. Hematoxylin was added as a counterstain for approximately 20 seconds, and the sections were dehydrated in increasing concentrations of ethyl alcohol (2$\times$ each at 70%, 80%, 95%, and 100%). Coverslips were mounted using permount mounting medium (#SP15-100; Fisher, Hampton, NH) in xylene. Serial sections were processed for routine histology (H&E).

Figure 3. (***See previous page***). **Validation of specific peptide binding to claudin-1 with human CRC cells.** On confocal microscopy, RTS*-Cy5.5 showed different levels of binding to the cell surface (*arrow*) of (*A*) SW480, (*B*) SW620, and (*C*) HCT116 cells. (*D–F*) Minimal signal is observed for SPT*-Cy5.5 to each of the cells. (*G*) RTS*-Cy5.5 showed higher fluorescence intensities than SPT*-Cy5.5 on binding to SW480 and SW620 cells with a 7.8 and 4.3 average fold-change ($P = 2 \times 10^{-5}$ and 4×10^{-4}) respectively. A small nonsignificant increase was observed for HCT116 cells with a 0.64 average fold-change ($P = .19$). The differences between RTS*-Cy5.5 and SPT*-Cy5.5 were significantly larger for SW480 and SW620 than the same difference for HCT116 with 12.3 and 6.8 average fold-change ($P = 10^{-4}$ and 10^{-3}), respectively. We fit a 1-way analysis of variance model to log-transformed data with terms for the means of 6 conditions, testing for RTS*-Cy5.5 vs SPT*-Cy5.5 and the difference of those differences between the cell lines. Measurements are an average of 10 randomly chosen cells from each of 3 slides for each condition. (*H*) Western blot shows claudin-1 expression in the cytoplasmic fraction (C) and on the plasma membrane (M) for each cell. Confocal fluorescence images show strong binding of (*I*) RTS*-Cy5.5 peptide (red) and (*J*) AF488-labeled anti-CLDN1 antibody (green) to the surface (*arrow*) of control SW620 cells (transfected with nontargeting siRNA, siCL). (*K*) Binding by the SPT*-Cy5.5 (red) control peptide is minimal. (*L–N*) The fluorescence intensities were reduced significantly in knockdown SW620 cells transfected with CLDN1-targeted siRNA, siCLDN1. (*O*) We fit a 2-way analysis of variance model with terms for siRNA type (knockdown and control) and targeting moieties (RTS*-Cy5.5, anti-CLDN1, and SPT*-Cy5.5) and their interactions to the average intensities on each slide (10 cells per slide with 2 slides per condition). The signal for RTS*-Cy5.5 decreased more than 10-fold with siRNA knockdown of CLDN1 ($P = 2 \times 10^{-7}$), which was a significantly larger decrease than the same difference for the control peptide ($P = 10^{-6}$). The antibody signal also decreased significantly ($P = 5 \times 10^{-7}$). (*P*) Western blot shown for control (siCL) and knockdown (siCLDN1) SW620 cells.

Immunofluorescence of Proximal Human Colon With Claudin-1 Peptide and Antibody

Formalin-fixed, paraffin-embedded specimens of adenomas, sessile serrated adenomas, hyperplastic polyps, and normal colonic mucosa from human proximal colon were obtained from the archived tissue bank in the Department of Pathology. Sections (5-μm thick) were cut and mounted onto glass slides (Superfrost Plus; Fischer Scientific). The tissues were deparaffinized, and antigen retrieval was performed as described earlier. The sections were blocked with protein serum for 15 minutes at RT followed by rinsing with PBS. The sections then were stained with RTS*-Cy5.5 at a 5-μmol/L concentration for 10 minutes at RT. The sections then were washed 3× with PBS (3 minutes each) and incubated overnight with (1:200) anti–claudin-1 antibody (clone Jay.8; Invitrogen). The sections were washed 3× with PBST, and incubated with (1:500) goat anti-rabbit antibody labeled with AF488 (Invitrogen) for 1 hour at RT. The sections were washed again 3× with PBST and mounted with Prolong Gold reagent containing DAPI (Invitrogen) using #1 cover glass (1.5-μm thickness). The images were collected with the same exposure time for all specimens. We placed 3 boxes with dimensions of 20 × 20 μm^2 completely within colonic epithelium in each image, and measured the mean fluorescence intensities for RTS*-Cy5.5 using custom Matlab software. Regions of saturated intensities were avoided. The results were transformed in base-2 log to improve normality and stabilize variance, and then fit with a 1-way analysis of variance model. Adjacent sections were processed for routine histology (H&E), and reviewed by 2 gastrointestinal pathologists (S.R.O. and H.D.A.).

All authors had access to the study data, and reviewed and approved the final manuscript.

Results

Identification of Claudin-1 Target

In the GSE41258 data set,[29] we found a 2.5-fold increase in gene expression for claudin-1 in human colonic adenomas (n = 45) compared with normal mucosa (n = 52) (Figure 1*A*). On immunohistochemistry (IHC), we evaluated expression of this protein target in archived human specimens from the proximal colon. Figure 1*B* and *C* show minimal staining for the representative sections of normal and hyperplastic polyps. Figure 1*D* and *E* show intense cell surface staining for representative sections of SSAs and adenomas. Consensus between 2 gastrointestinal pathologists (S.R.O. and H.D.A.) using a standard IHC scoring system showed overexpression, defined by either 2+ or 3+ staining, in 14% (4 of 28) of normal, 17% (2 of 12) of hyperplastic polyps, 73% (8 of 11) of SSAs, and 87% (26 of 30) of adenomas. These results support claudin-1 as a promising early target for the detection of proximal colon cancers.

Identification of a Peptide Specific for Claudin-1

Figure 2*A* shows the structure of claudin-1 on the cell surface. We used the 53-80 amino acid loop of the extracellular domain as the biopanning substrate for peptide selection with phage display. After 3 rounds, we found the peptide sequence RTSPSSR to be highly enriched with expression in 43 of 50 of clones. Figure 2*B* shows the synthesized peptide (black) labeled with Cy5.5 (red) via a GGGSK linker (blue) on the C-terminus to prevent steric hindrance. Cy5.5 was chosen for use as the label because of its high quantum yield and photostability.[48] Figure 2*C* shows the scrambled sequence SPTSSRR used for control. Figure 2*D* shows the fluorescence spectra of RTS*-Cy5.5 and SPT*-Cy5.5 with a peak emission in the near-infrared spectrum at λ_{em} = 710 nm using excitation at λ_{ex} = 671 nm. We purified the Cy5.5-labeled peptides to more than 95% on high-performance liquid chromatography, and measured an experimental mass-to-charge ratio of 1740.9 for RTS*-Cy5.5 on mass spectrometry, which agrees with the expected value (Figure 2*E*).

Immunocytochemistry

On confocal microscopy, we examined cells with either high (SW620, SW480) or low (HCT116) claudin-1 expression to validate specific binding of the RTS*-Cy5.5 peptide to the plasma membrane. We found greater amounts of RTS*-Cy5.5 bound to the surface (arrows) of SW480 and SW620 cells compared with HCT116 cells (Figure 3*A–C*), whereas the SPT*-Cy5.5 control showed minimal binding to all cells (Figure 3*D–F*). Figure 3*G* shows quantified fluorescence intensities for RTS*-Cy5.5 to be significantly greater than that for SPT*-Cy5.5 to SW480 and SW620, but not to HCT116 cells. In addition, the RTS*-Cy5.5 vs SPT*-Cy5.5 differences were significantly greater for SW480 and SW620 than for HCT116. Western blot confirmed higher claudin-1 expression for SW480 and SW620 than for HCT116 cells on the plasma membrane (Figure 3*H*). Claudin-1 expression in the cytoplasmic fraction of each cell line was relatively low compared with the cell surface.

siRNA Knockdown of Claudin-1 Expression

We performed siRNA knockdown experiments with SW620 cells to support specific binding of the RTS*-Cy5.5 peptide to claudin-1. We found that RTS*-Cy5.5 and AF488-labeled anti-CLDN1 antibody show strong binding to the surface of SW620 cells transfected with a control siRNA (siCL) (Figure 3*I* and *J*), and reduced binding to cells transfected with siCLDN1-targeted siRNA (Figure 3*L* and *M*). SPT*-Cy5.5 produced minimal binding with either siRNA (Figure 3*K* and *N*). Figure 3*O* shows quantified fluorescence intensities for RTS*-Cy5.5 to a decrease more than 10-fold with CLND1 siRNA knockdown compared with the control knockdown, which was significantly greater than the decrease in signal for SPT*-Cy5.5 (control). Signal from anti-CLDN1 also decreased significantly, showing an effective knockdown. Western blot confirmed the high expression of claudin-1 in SW620 cells as well as for the cells transfected with control siRNA, whereas expression was reduced by approximately 44% for cells transfected with siCLDN1 (Figure 3*P*).

Competition for Peptide Binding

We evaluated binding of RTS*-Cy5.5 to SW620 cells with competition from unlabeled RTS* and SPT* peptides to

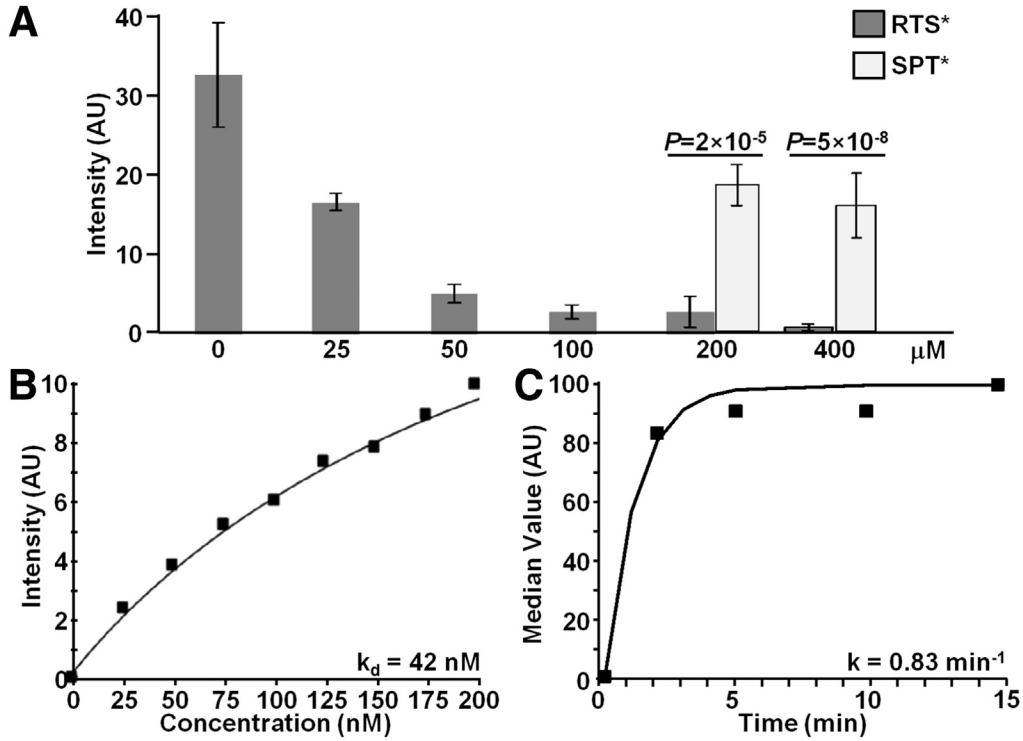

Figure 4. Characterization of claudin-1 peptide binding. (*A*) On competition, RTS*-Cy5.5 showed less binding to SW620 cells with addition of unlabeled RTS* at concentrations of 25 μmol/L and higher compared with a concentration of 0 μmol/L. With unlabeled RTS* at concentrations of 200 and 400 umol/L, the signal from RTS*-Cy5.5 was significantly lower than that measured when competing with unlabeled SPT* at the same concentrations ($P < 2 \times 10^{-5}$). Analysis was performed using an analysis of variance model with terms for 8 means fit to log-transformed data. Measurements are an average of 10 randomly chosen cells on each of 3 slides at each condition for RTS* and 2 slides for each condition for SPT*. (*B*) We measured an apparent dissociation constant (binding affinity) of $k_d = 42$ nmol/L and $R^2 = 0.95$ for RTS*-Cy5.5 to SW620 cells. (*C*) We measured an apparent association time constant of $k = 0.83$ min^{-1}, which corresponds to less than 1.2 minutes. Results for each measurement are representative of 2 independent experiments.

support specific binding by the RTS* peptide rather than the Cy5.5 label. Figure 4*A* shows that the addition of 25, 50, 100, 200, and 400 μmol/L of unlabeled RTS* produces a dose-dependent reduction in fluorescence intensity of RTS*-Cy5.5 using confocal microscopy. By comparison, addition of unlabeled SPT* at the higher concentrations of 200 and 400

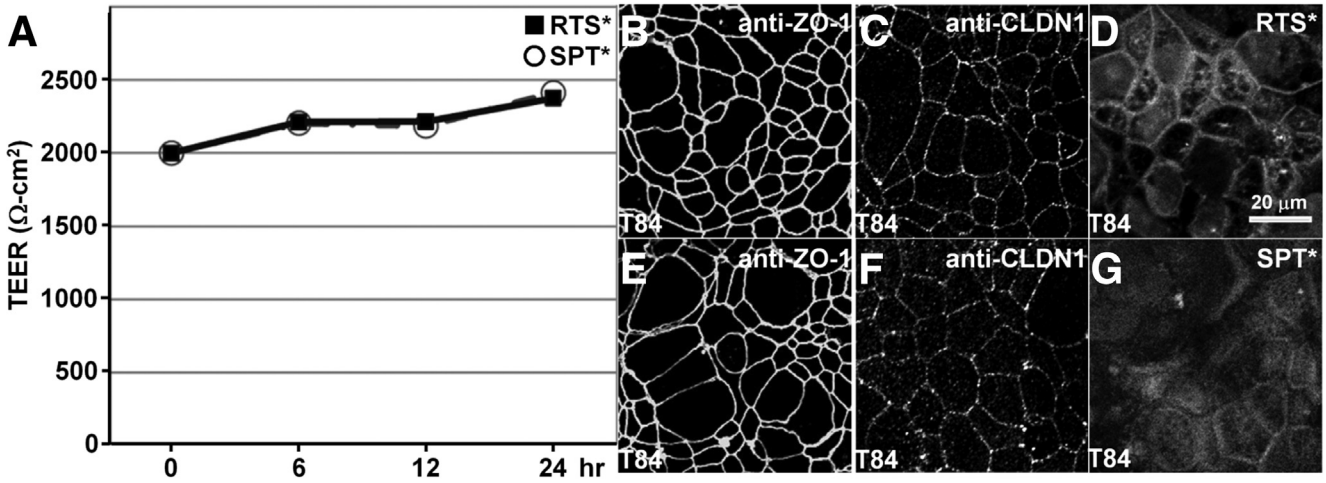

Figure 5. Tight junction function and ZO-1 distribution are not altered by claudin-1 peptide. (*A*) Confluent T84 monolayers were incubated with either 5 μmol RTS* or SPT* (control), peptides show high TEER for up to 24 hours. Immunofluorescence shows localization of (*B* and *E*) anti–ZO-1 and (*C* and *F*) anti-CLDN1 antibodies on the apical plasma membrane of tight junctions at 24 hours after peptide incubation. (*D*) RTS* peptide partially localizes to cellular junctions.

μmol/L showed a significantly higher RTS*-Cy5.5 fluorescence intensity than with equivalent concentrations of unlabeled RTS*.

Characterization of Peptide Binding

We performed flow cytometry experiments with SW620 cells to characterize peptide binding parameters. Figure 4*B* shows an apparent dissociation constant for the RTS*-Cy5.5 peptide of $k_d = 42$ nmol/L and $R^2 = 0.95$. This result provides a measure of binding affinity. Figure 4*C* shows an apparent association time constant of $k = 0.83$ min^{-1} for RTS*-Cy5.5. This result provides a time scale of approximately 1.2 minutes for binding with topical administration.

TEER Measurements

We evaluated the effect of peptide binding on tight junction function using a polarized monolayer of T84 cells plated on Transwell supports. We found high TEER with either RTS* or SPT* for up to 24 hours (Figure 5*A*). On immunofluorescence, we observed antibodies for ZO-1 (Figure 5*B* and *E*), and claudin-1 (Figure 5*C* and *F*), to localize to the cell junctions. These results show that neither peptide alters tight junction function or ZO-1 distribution. The RTS* peptide localizes partially to cellular junctions by comparison with SPT* (Figure 5*D* and *G*).

Validation of Claudin-1 Expression in Mouse Colon

We performed IHC and immunofluorescence (IF) to show overexpression of claudin-1 in dysplasia compared with normal in resected specimens of colon from the *CPC;Apc* mouse. Figure 6*A* and *B* show intense staining using the anti–claudin-1 antibody for dysplasia on IHC and IF, respectively, whereas Figure 6*D* and *E* show minimal signal for normal colonic mucosa on IHC and IF. Figure 6*C* and *F* show corresponding histology (H&E) for dysplasia and normal, respectively.

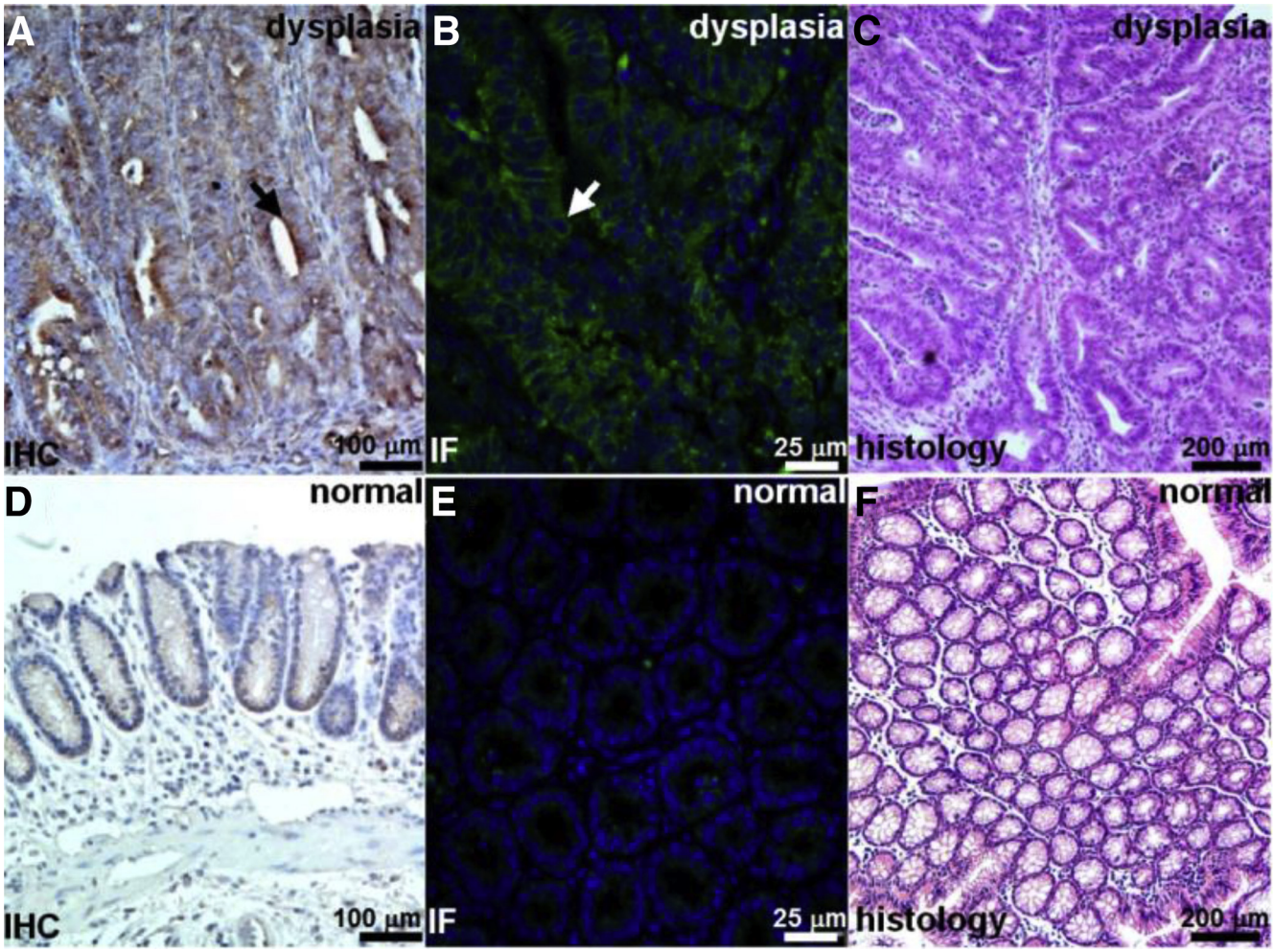

Figure 6. Increased claudin-1 expression in *CPC;Apc* mouse colonic adenomas. Strong staining of claudin-1 in dysplasia is seen with (*A*) IHC and (*B*) IF using AF488 label. (*C*) Representative histology (H&E) for dysplasia. Minimal expression of claudin-1 was observed in normal colonic mucosa on (*D*) immunohistochemistry and (*E*) immunofluorescence. (*F*) Representative histology (H&E) for normal.

In Vivo Imaging in Mouse Colon

We used a small-animal endoscope to compare binding between the claudin-1 and control peptides in 5 *CPC;Apc* mice. After collecting white-light images, either RTS*-Cy5.5 or SPT*-Cy5.5 was administered intrarectally, and was allowed to incubate for 5 minutes. The unbound peptides then were rinsed away. On in vivo white-light images, Figure 7*A* and *B* (Video 1) show a sporadic polyp (arrow), and Figure 7*C* shows apparent normal colonic mucosa with no grossly visible adenomas. On the corresponding

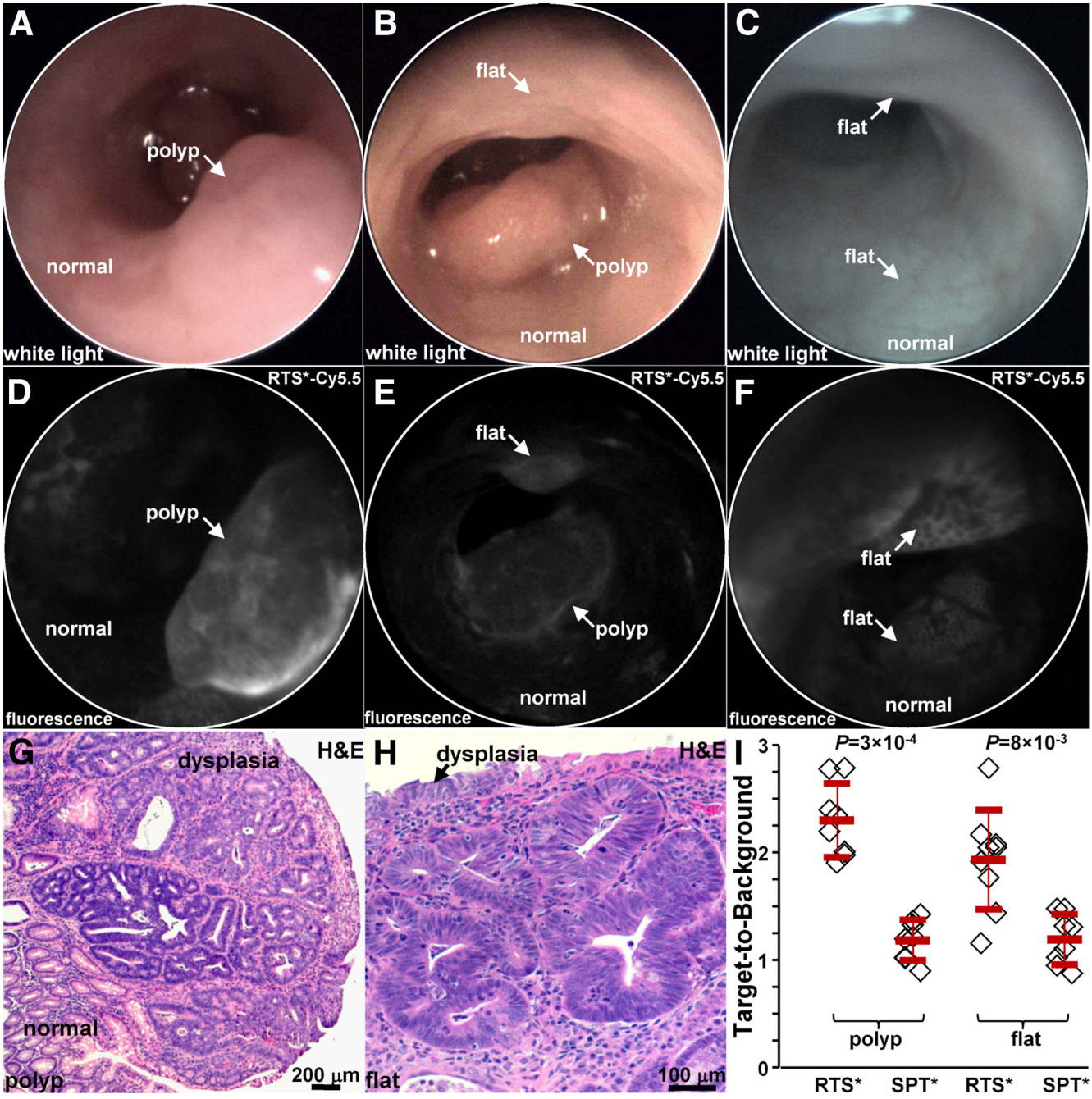

Figure 7. In vivo imaging in *CPC;Apc* mouse colon. White-light images show (*A* and *B*) a spontaneous polyp (*arrow*) and (*C*) normal-appearing mucosa. Near-infrared fluorescence images after topical administration of RTS*-Cy5.5 shows (*D*) increased intensity from the polyp (*arrow*) in panel *A*, (*E*) presence of a flat lesion above the polyp in panel *B*, and (*F*) flat lesions not apparent on the white-light image in panel *C*. Representative individual images were extracted from videos recorded at 15 frames per second, which showed minimum motion artifact and absence of debris (stool, mucus). Histology (H&E) of (*G*) the polyp in panel *A* and (*H*) the flat lesion in panel *B* shows features of low-grade dysplasia. (*I*) From 5 mice, RTS*-Cy5.5 had a higher mean (±SD) T/B ratio than SPT*-Cy5.5 for 8 polyps (2.3 ± 0.3 and 1.2 ± 0.2, respectively; $P = 3\times10^{-4}$ by paired *t* test) and 9 flat lesions (1.9 ± 0.5 and 1.1 ± 0.2, respectively; $P = 8 \times 10^{-3}$ by paired *t* test).

fluorescence images after administration of RTS*-Cy5.5, Figure 7*D* shows increased intensity from the polyp in a heterogeneous pattern, whereas normal colonic mucosa shows minimal background. Figure 7*E* shows the presence of a flat lesion above the polyp that is not apparent on the white-light image in Figure 7*B* that was found later on pathology to be dysplasia (Video 2). Figure 7*F* shows 2 flat regions of increased fluorescence intensity that were confirmed to be dysplasia on pathology. The staining pattern appears to outline dysplastic crypts.

After completion of imaging, the mice were euthanized. The colon was excised and the mucosal surface was exposed to identify polyps. White-light and fluorescence images were collected from each specimen using Xenogen IVIS Spectrum (Perkin Elmer, Waltham, MA). Regions of increased intensity were registered with the endoscopic images using landmarks defined by distance from the anus and clockwise location, and submitted for histology. The pathologist identified 8 polyps and 9 flat lesions. Figure 7*G* shows the histology of a polyp with features of low-grade dysplasia, including collections of irregular crypts lined by epithelium with crowded, elongated, and hyperchromatic nuclei. Figure 7*H* shows the histology of a flat lesion with similar histologic features of dysplasia. We found a significantly greater mean T/B ratio for RTS*-Cy5.5 than for SPT*-Cy5.5 for both polyps and flat lesions (Figure 7*I*).

We then compared binding of the claudin-1 peptide between dysplasia and normal colonic mucosa in 3 mice at 10 weeks of age when they first begin to form polyps. We administered RTS*-Cy5.5 in vivo. After euthanizing the mice, we collected white-light (Figure 8*A*) and near-infrared fluorescence images (Figure 8*B*) from the excised colon specimens. The tissues were sectioned along planes parallel to the surface, and the pathologist (S.R.O.) identified regions of dysplasia (red) and normal (blue) on histology (Figure 8*C*) while blinded to the imaging results. Magnified regions of normal and dysplasia are shown in Figure 8*D* and *E*, respectively. The pathologist identified a total of 9 regions of dysplasia and 7 sites of normal. The intensities from these regions were measured from the fluorescence images. We found a significantly greater T/B ratio for dysplasia compared with normal (Figure 8*F*).

Binding of Claudin-1 Peptide to Human Proximal Colonic Lesions

We show the potential for clinical translation of this peptide by examining specific binding on formalin-fixed, paraffin-embedded specimens of human proximal colon. On confocal microscopy, we observed minimal fluorescence intensity for both RTS*-Cy5.5 (red) and AF488-labeled anti-CLDN1 antibody (green) on representative specimens of human normal and hyperplastic polyps, respectively (Figure 9*A* and *B*). By comparison, we observed bright fluorescence from representative specimens of SSAs and adenomas (Figure 9*C* and *D*, respectively). These results show strong binding of the RTS*-Cy5.5 peptide to claudin-1

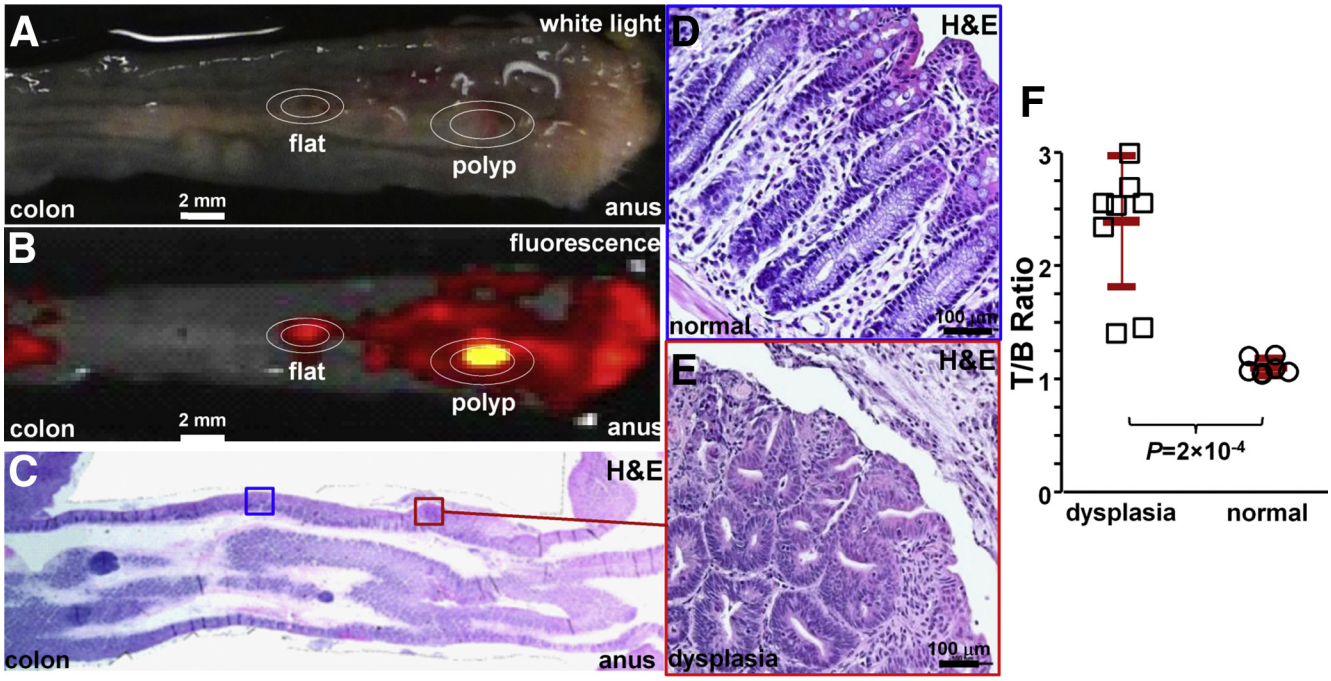

Figure 8. Ex vivo validation of peptide binding to colonic dysplasia. (*A*) Representative white-light image of excised distal 2 cm of mouse colonic mucosa accessed by endoscopy after RTS*-Cy5.5 was administered topically in vivo. (*B*) Near-infrared image shows regions of increased fluorescence intensity. (*C*) Histology (H&E) sectioned parallel to mucosal surface was evaluated for the presence of dysplasia by an expert gastrointestinal pathologist (S.R.O.). Expanded views of (*D*) normal and (*E*) dysplasia (original magnification: 20×). (*F*) From 3 mice, the mean (±SD) T/B ratio was significantly higher for 9 regions of dysplasia compared with 7 normal (2.4 ± 0.6 vs 1.1 ± 0.1, respectively; $P = 2 \times 10^{-4}$ by unpaired *t* test).

at the cell surface (arrows) of SSAs and adenomas. We measured the fluorescence intensities from binding of the RTS*-Cy5.5 peptide in a set of 3 boxes with dimensions of 20×20 μm^2 located at random on cells in the epithelium. We found greater mean intensities for adenomas vs normal and hyperplastic polyps and for SSAs vs normal and hyperplastic polyps. Figure 8*E* shows a mean fold-difference of 2.8 and 2.2 for adenomas and SSAs vs normal, respectively.

Discussion

On gene expression profiles, we found claudin-1 to be overexpressed in human colonic adenomas by 2.54-fold compared with normal mucosa. This result was confirmed by expression of the protein target in 73% (8 of 11) of SSAs and in 87% (26 of 30) of adenomas from the proximal human colon on immunohistochemistry. Significantly reduced staining of this cell surface target was observed in hyperplastic polyps and normal mucosa. Because claudin-1 is expressed early in the development of CRC, it may be useful for detecting either polypoid or flat precancerous lesions that are difficult to visualize.[13] We identified the peptide RTSPSSR, and showed that it binds specifically to claudin-1 in knockdown and competition experiments. We found this peptide to have adequate binding affinity of $k_d = 42$ nmol/L and rapid binding within less than 1.2 minutes ($k = 0.83$ min^{-1}) with topical administration in vivo. We showed specific peptide binding to spontaneous colonic adenomas in mice that were either polypoid or flat in morphology. Finally, we found significantly greater fluorescence intensity from peptide binding to SSAs and

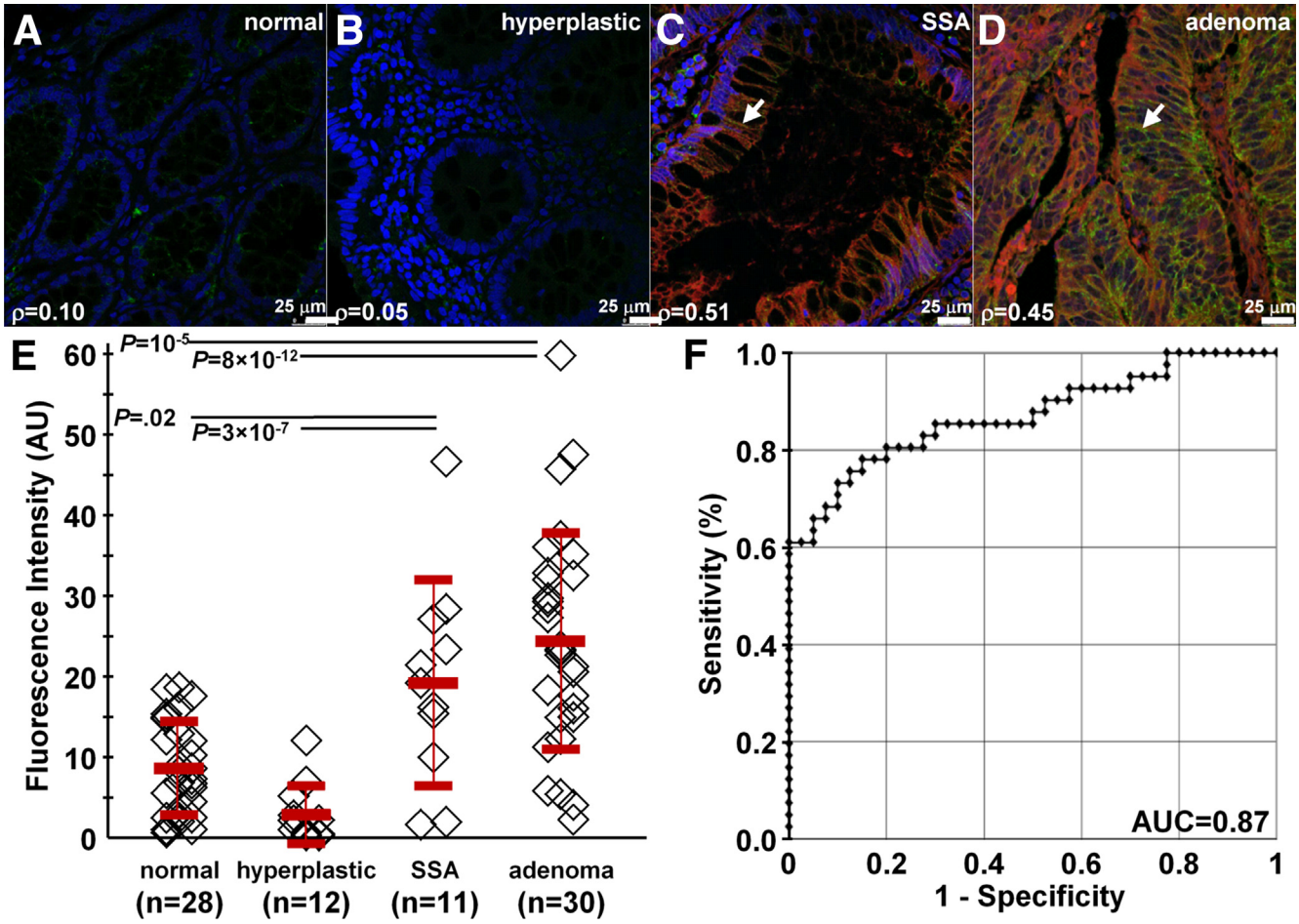

Figure 9. Binding of claudin-1 peptide to human proximal colonic neoplasia. On confocal microscopy, there was minimal binding of RTS*-Cy5.5 peptide (red) and AF488-labeled anti–claudin-1 antibody (green) to human (*A*) normal colonic mucosa and (*B*) hyperplastic polyps. DAPI (blue) identifies nuclei. Strong staining with both peptide and antibody was observed for representative specimens of (*C*) SSAs and (*D*) adenomas from the proximal colon. The extent of co-localization of peptide and antibody binding is characterized by the Pearson correlation coefficient ρ. Representative images were selected from 28 normal, 12 hyperplastic polyps, 11 SSAs, and 30 adenomas. (*E*) We found a significantly greater mean (±SD) intensity for adenomas (25.5 ± 14.0) vs normal (9.1 ± 6.0) and hyperplastic polyps (3.1 ± 3.7) ($P = 10^{-5}$ and 8×10^{-12}, respectively), as well as for SSAs (20.1 ± 13.3) vs normal and hyperplastic polyps ($P = .02$ and 3×10^{-7}, respectively). Analysis of variance models (ANOVA) were used with means for 4 groups, fit to log-transformed data. The fluorescence intensities from 3 boxes (20×20 μm^2) located randomly on cells within each specimen were measured and averaged. (*F*) The receiver operator characteristic curve shows an area under the curve (AUC) of 0.87.

adenomas from human proximal colon compared with normal and hyperplastic polyps.

Although widespread use of colonoscopy has resulted in a reduced incidence and mortality from CRC, this procedure has been shown to be much less effective than expected.[4–12] Cases of CRC diagnosed after colonoscopy are common, and as many as 1 in 10 CRCs are found in patients who have completed this procedure.[49–51] Although interval cancers may occur for a variety of reasons, most tumors are thought to arise from prevalent lesions that were missed by colonoscopy. Efforts to improve quality have focused on increasing instrument withdrawal time, adenoma detection rate, and bowel preparation quality.[52] However, reports of interval cancers in subjects undergoing careful endoscopic examination in clinical studies have shown that conventional white-light colonoscopy can be ineffective even under optimal conditions.[53,54] Advanced endoscopic techniques such as narrow-band imaging[55–57] and chromoendoscopy[58–60] are being investigated to improve polyp visualization, but these technologies are limited by nonspecific detection mechanisms and have not shown improvement in the adenoma detection rate or in patient outcomes.[61,62] Thus, a targeted approach, such as with use of peptides, may be more effective.

Use of fluorescently labeled imaging agents that are specific for early targets may improve cancer surveillance in high-risk populations, such as those with multiple polyps, a family history of CRC, Lynch syndrome, or inflammatory bowel disease.[63,64] In particular, premalignant lesions found sporadically in the proximal colon may be more difficult to detect because of a flat appearance. Multimodal endoscopes that are sensitive to either white light or fluorescence have been developed for clinical use.[65] A peptide specific for c-Met and labeled with Cy5 recently was used in human beings with intravenous administration.[66] An increase in fluorescence was found for adenomas with either polypoid or flat morphology on back-to-back examinations using white light alone followed by white light with peptide. With topical administration, peptides can be delivered in high concentrations directly to mucosa at risk of harboring disease to maximize binding interactions and achieve high image contrast with little risk for toxicity. This approach results in rapid and predictable binding with minimal background, and avoids undesired biodistribution of the exogenous agent to other tissues, such as what occurs with intravenous administration. Because of their small size, peptides have reduced immunogenicity and lower costs than antibodies for mass manufacture. This method of contrast application is similar to that used in chromoendoscopy, which is now recommended by an international panel of experts for cancer surveillance in patients with ulcerative colitis,[67] but with the added benefit of molecular specificity.

Future development of this peptide will require in vivo clinical validation in human studies. Although we found promising results with this peptide alone, disease heterogeneity in a broad patient population may require use of additional targets using multiplexed imaging methods.[40] We previously showed a peptide VRPMPLQ that was identified from human colonic polyps obtained via biopsy using phage display.[36] This peptide was labeled with fluorescein isothiocyanate, and specific binding was validated in vivo on dysplastic polyps with confocal endomicroscopy.[36] Because this peptide was selected empirically, the target is unknown and its clinical use may not be widely generalizable. Our claudin-1 peptide, on the other hand, was selected based on a known target identified from a human gene expression data set. Furthermore, this peptide can be used in a multimer configuration to detect multiple targets concurrently and potentially detect disease at lower levels of molecular expression.[41] Claudin-1 is overexpressed in human colonic adenomas, and represents a promising early target for detection of CRC using a near-infrared, labeled fluorescence peptide.

References

1. Ferlay J, Shin HR, Bray F, et al. Estimates of worldwide burden of cancer in 2008: GLOBOCAN 2008. Int J Cancer 2010;127:2893–2917.
2. Levine JS, Ahnen DJ. Clinical practice. Adenomatous polyps of the colon. N Engl J Med 2006;355:2551–2557.
3. Seeff LC, Richards TB, Shapiro JA, et al. How many endoscopies are performed for colorectal cancer screening? Results from CDC's survey of endoscopic capacity. Gastroenterology 2004;127:1670–1677.
4. Heresbach D, Barrioz T, Lapalus MG, et al. Miss rate for colorectal neoplastic polyps: a prospective multicenter study of back-to-back video colonoscopies. Endoscopy 2008;40:284–290.
5. Rex DK, Cutler CS, Lemmel GT, et al. Colonoscopic miss rates of adenomas determined by back-to-back colonoscopies. Gastroenterology 1997;112:24–28.
6. O'Brien MJ, Winawer SJ, Zauber AG, et al; National Polyp Study Workgroup. Flat adenomas in the National Polyp Study: is there increased risk for high-grade dysplasia initially or during surveillance? Clin Gastroenterol Hepatol 2004;2:905–911.
7. Nishihara R, Wu K, Lochhead P, et al. Long-term colorectal-cancer incidence and mortality after lower endoscopy. N Engl J Med 2013;369:1095–1105.
8. Singh H, Nugent Z, Demers AA, et al. The reduction in colorectal cancer mortality after colonoscopy varies by site of the cancer. Gastroenterology 2010;139:1128–1137.
9. Baxter NN, Goldwasser MA, Paszat LF, et al. Association of colonoscopy and death from colorectal cancer. Ann Intern Med 2009;150:1–8.
10. Lakoff J, Paszat LF, Saskin R, et al. Risk of developing proximal versus distal colorectal cancer after a negative colonoscopy: a population-based study. Clin Gastroenterol Hepatol 2008;6:1117–1121.
11. Bressler B, Paszat LF, Chen Z, et al. Rates of new or missed colorectal cancers after colonoscopy and their risk factors: a population-based analysis. Gastroenterology 2007;132:96–102.
12. Singh H, Turner D, Xue L, et al. Risk of developing colorectal cancer following a negative colonoscopy examination: evidence for a 10-year interval between colonoscopies. JAMA 2006;295:2366–2373.

13. Rondagh EJ, Bouwens MW, Riedl RG, et al. Endoscopic appearance of proximal colorectal neoplasms and potential implications for colonoscopy in cancer prevention. Gastrointest Endosc 2012;75:1218–1225.
14. Rembacken BJ, Fujii T, Cairns A, et al. Flat and depressed colonic neoplasms: a prospective study of 1000 colonoscopies in the UK. Lancet 2000; 8:1211–1214.
15. le Clercq CM, Bouwens MW, Rondagh EJ, et al. Postcolonoscopy colorectal cancers are preventable: a population-based study. Gut 2014;63:957–963.
16. Bond JH. Polyp guideline: diagnosis, treatment, and surveillance for patients with colorectal polyps. Practice Parameters Committee of the American College of Gastroenterology. Am J Gastroenterol 2000;95: 3053–3063.
17. Patil DT, Shadrach BL, Rybicki LA, et al. Proximal colon cancers and the serrated pathway: a systematic analysis of precursor histology and BRAF mutation status. Mod Pathol 2012;25:1423–1431.
18. Mrsny RJ, Brown GT, Gerner-Smidt K, et al. A key claudin extracellular loop domain is critical for epithelial barrier integrity. Am J Pathol 2008;172:905–915.
19. Dhawan P, Singh AB, Deane NG, et al. Claudin-1 regulates cellular transformation and metastatic behavior in colon cancer. J Clin Invest 2005;115:1765–1776.
20. Miwa N, Furuse M, Tsukita S, et al. Involvement of claudin-1 in the beta-catenin/Tcf signaling pathway and its frequent upregulation in human colorectal cancers. Oncol Res 2001;12:469–476.
21. de Oliveira SS, de Oliveira IM, De Souza W, et al. Claudins upregulation in human colorectal cancer. FEBS Lett 2005;579:6179–6185.
22. Ersoz S, Mungan S, Cobanoglu U, et al. Prognostic importance of claudin-1 and claudin-4 expression in colon carcinomas. Pathol Res Pract 2011;207:285–289.
23. Iacobuzio-Donahue CA, Maitra A, Shen-Ong GL, et al. Discovery of novel tumor markers of pancreatic cancer using global gene expression technology. Am J Pathol 2002;160:1239–1249.
24. Lee JW, Lee SJ, Seo J, et al. Increased expressions of claudin-1 and claudin7 during the progression of cervical neoplasia. Gynecol Oncol 2005;97:53–59.
25. Morita K, Tsukita S, Miyachi Y. Tight junction-associated proteins (occludin, ZO-1, claudin-1, claudin4) in squamous cell carcinoma and Bowen's disease. Br J Dermatol 2004;151:328–334.
26. Resnick MB, Gavilanez M, Newton E, et al. Claudin expression in gastric adenocarcinomas: a tissue microarray study with prognostic correlation. Hum Pathol 2005;36:886–892.
27. Hsueh C, Chang YS, Tseng NM, et al. Expression pattern and prognostic significance of claudins 1, 4, and 7 in nasopharyngeal carcinoma. Hum Pathol 2010;41: 944–950.
28. Fluge Ø, Bruland O, Akslen LA, et al. Gene expression in poorly differentiated papillary thyroid carcinomas. Thyroid 2006;16:161–175.
29. Sheffer M, Bacolod MD, Zuk O, et al. Association of survival and disease progression with chromosomal instability: a genomic exploration of colorectal cancer. Proc Natl Acad Sci U S A 2009;106:7131–7136.
30. Caruso M, Fung KY, Moore J, et al. Claudin-1 expression is elevated in colorectal cancer precursor lesions harboring the BRAF V600E mutation. Transl Oncol 2014;7:456–463.
31. Kinugasa T, Huo Q, Higashi D, et al. Selective upregulation of claudin-1 and claudin-2 in colorectal cancer. Anticancer Res 2007;27:3729–3734.
32. Gröne J, Weber B, Staub E, et al. Differential expression of genes encoding tight junction proteins in colorectal cancer: frequent dysregulation of claudin-1, 8 and 12. Int J Colorectal Dis 2007;22:651–659.
33. Mees ST, Mennigen R, Spieker T, et al. Expression of tight and adherens junction proteins in ulcerative colitis associated colorectal carcinoma: upregulation of claudin-1, claudin-3, claudin-4, and beta-catenin. Int J Colorectal Dis 2009;24:361–368.
34. Weber CR, Nalle SC, Tretiakova M, et al. Claudin-1 and claudin-2 expression is elevated in inflammatory bowel disease and may contribute to early neoplastic transformation. Lab Invest 2008;88:1110–1120.
35. Kinugasa T, Akagi Y, Yoshida T, et al. Increased claudin-1 protein expression contributes to tumorigenesis in ulcerative colitis-associated colorectal cancer. Anticancer Res 2010;30:3181–3186.
36. Hsiung P, Hardy J, Friedland S, et al. Detection of colonic dysplasia in vivo using a targeted heptapeptide and confocal microendoscopy. Nat Med 2008;14:454–458.
37. Sturm MB, Joshi BP, Lu S, et al. Targeted endoscopic imaging of Barrett's neoplasia with specific fluorescent-labeled peptide: first in-human results. Sci Transl Med 2013;5:184ra61.
38. Sturm MB, Piraka C, Elmunzer BJ, et al. In vivo molecular imaging of Barrett's esophagus with confocal laser endomicroscopy. Gastroenterology 2013;145:56–58.
39. Li M, Anastassiades CP, Joshi B, et al. Affinity peptide for targeted detection of dysplasia in Barrett's esophagus. Gastroenterology 2010;139:1472–1480.
40. Joshi BP, Miller SJ, Lee CM, et al. Multispectral endoscopic imaging of colorectal dysplasia in vivo. Gastroenterology 2012;143:1435–1437.
41. Joshi BP, Liu Z, Elahi SF, et al. Near-infrared-labeled peptide multimer functions as phage-mimic for high affinity, specific targeting of colonic adenomas in vivo. Gastrointest Endosc 2012;76:1197–1206.
42. Thomas R, Chen J, Roudier MM, et al. In vitro binding evaluation of 177Lu-AMBA, a novel 177Lu-labeled GRP-R agonist for systemic radiotherapy in human tissues. Clin Exp Metastasis 2009;26:105–119.
43. Liu Y, Nusrat A, Schnell FJ, et al. Human junction adhesion molecule regulates tight junction resealing in epithelia. J Cell Sci 2000;113:2363–2374.
44. Fan S, Fogg V, Wang Q, et al. A novel Crumbs3 isoform regulates cell division and ciliogenesis via importin beta interactions. J Cell Biol 2007;178:387–398.
45. Hinoi T, Akyol A, Theisen BK, et al. Mouse model of colonic adenoma-carcinoma progression based on somatic Apc inactivation. Cancer Res 2007;67:9721–9730.
46. Rowan AJ, Lamlum H, Ilyas M, et al. APC mutations in sporadic colorectal tumors: a mutational "hotspot" and

interdependence of the "two hits". Proc Natl Acad Sci U S A 2000;97:3352–3357.
47. Zhou J, Joshi BP, Duan X, et al. EGFR overexpressed in colonic neoplasia can be detected on wide-field endoscopic imaging. Clin Transl Gastroenterol 2015;6:e101.
48. Luo S, Zhang E, Su Y, et al. A review of NIR dyes in cancer targeting and imaging. Biomaterials 2011;32:7127–7138.
49. Sanduleanu S, Masclee AM, Meijer GA. Interval cancers after colonoscopy-insights and recommendations. Nat Rev Gastroenterol Hepatol 2012;9:550–554.
50. Robertson DJ, Lieberman DA, Winawer SJ, et al. Colorectal cancers soon after colonoscopy: a pooled multicohort analysis. Gut 2014;63:949–956.
51. Farrar WD, Sawhney MS, Nelson DB, et al. Colorectal cancers found after a complete colonoscopy. Clin Gastroenterol Hepatol 2006;4:1259–1264.
52. Rex DK, Schoenfeld PS, Cohen J, et al. Quality indicators for colonoscopy. Am J Gastroenterol 2015;110:72–90.
53. Shergill AK, Conners EE, McQuaid KR, et al. Protective association of colonoscopy against proximal and distal colon cancer and patterns in interval cancer. Gastrointest Endosc 2015;82:529–537 e1.
54. le Clercq CM, Winkens B, Bakker CM, et al. Metachronous colorectal cancers result from missed lesions and non-compliance with surveillance. Gastrointest Endosc 2015;82:325–333 e2.
55. Adler A, Aschenbeck J, Yenerim T, et al. Narrow-band versus white-light high definition television endoscopic imaging for screening colonoscopy: a prospective randomized trial. Gastroenterology 2009;136:410–416.e1; quiz 715.
56. East JE, Ignjatovic A, Suzuki N, et al. A randomized, controlled trial of narrow-band imaging vs high-definition white light for adenoma detection in patients at high risk of adenomas. Colorectal Dis 2012;14:e771–e778.
57. Pasha SF, Leighton JA, Das A, et al. Comparison of the yield and miss rate of narrow band imaging and white light endoscopy in patients undergoing screening or surveillance colonoscopy: a meta-analysis. Am J Gastroenterol 2012;107:363–370.
58. Kahi CJ, Anderson JC, Waxman I, et al. High-definition chromocolonoscopy vs. high-definition white light colonoscopy for average-risk colorectal cancer screening. Am J Gastroenterol 2010;105:1301–1307.
59. Lapalus MG, Helbert T, Napoleon B, et al. Does chromoendoscopy with structure enhancement improve the colonoscopic adenoma detection rate? Endoscopy 2006;38:444–448.
60. Le Rhun M, Coron E, Parlier D, et al. High resolution colonoscopy with chromoscopy versus standard colonoscopy for the detection of colonic neoplasia: a randomized study. Clin Gastroenterol Hepatol 2006;4:349–354.
61. Dinesen L, Chua TJ, Kaffes AJ. Meta-analysis of narrow-band imaging versus conventional colonoscopy for adenoma detection. Gastrointest Endosc 2012;75:604–611.
62. Rex DK, Clodfelter R, Rahmani F, et al. Narrow-band imaging versus white light for the detection of proximal colon serrated lesions: a randomized, controlled trial. Gastrointest Endosc 2016;83:166–171.
63. Kaminski MF, Hassan C, Bisschops R, et al. Advanced imaging for detection and differentiation of colorectal neoplasia: European Society of Gastrointestinal Endoscopy (ESGE) Guideline. Endoscopy 2014;46:435–449.
64. ASGE Standards of Practice CommitteeShergill AK, Lightdale JR, et al. The role of endoscopy in inflammatory bowel disease. Gastrointest Endosc 2015;81:1101–1121 e1–13.
65. Joshi BP, Duan X, Kwon RS, et al. Multimodal endoscope can quantify wide-field fluorescence detection of Barrett's neoplasia. Endoscopy 2016;48:1–15.
66. Burggraaf J, Kamerling IM, Gordon PB, et al. Detection of colorectal polyps in humans using an intravenously administered fluorescent peptide targeted against c-Met. Nat Med 2015;21:955–961.
67. Laine L, Kaltenbach T, Barkun A, et al. SCENIC Guideline Development Panel. SCENIC international consensus statement on surveillance and management of dysplasia in inflammatory bowel disease. Gastroenterology 2015;148:639–651.e28.

Received September 21, 2015. Accepted December 6, 2015.

Correspondence
Address correspondence to: Thomas D. Wang, MD, PhD, Division of Gastroenterology, University of Michigan, 109 Zina Pitcher Place, BSRB 1522, Ann Arbor, Michigan 48109-2200. e-mail: thomaswa@umich.edu; fax: (734) 647-7950.

Conflicts of interest
These authors disclose the following: Emily Rabinsky, Bishnu Joshi, and Thomas Wang are co-inventors on a patent application submitted by the University of Michigan on the peptide presented in this manuscript. The remaining authors disclose no conflicts.

Funding
Supported in part by National Institutes of Health grants R01 CA142750 (T.D.W.), R01 CA200007 (T.D.W.), and R01 EB020644 (T.D.W.), and gift funds provided by Mary L. Petrovich (T.D.W.).